Plant SMU-1 and SMU-2 Homologues Regulate Pre-mRNA Splicing and Multiple Aspects of Development[1][C][W][OA]

Taijoon Chung[2], Dongfang Wang, Cheol-Soo Kim[3], Ramin Yadegari, and Brian A. Larkins*

Department of Plant Sciences, University of Arizona, Tucson, Arizona 85721

In eukaryotes, alternative splicing of pre-mRNAs contributes significantly to the proper expression of the genome. However, the functions of many auxiliary spliceosomal proteins are still unknown. Here, we functionally characterized plant homologues of nematode *suppressors of mec-8 and unc-52* (*smu*). We compared transcript profiles of maize (*Zea mays*) *smu2* endosperm with those of wild-type plants and identified pre-mRNA splicing events that depend on the maize SMU2 protein. Consistent with a conserved role of plant SMU-2 homologues, Arabidopsis (*Arabidopsis thaliana*) *smu2* mutants also show altered splicing of similar target pre-mRNAs. The *Atsmu2* mutants occasionally show developmental phenotypes, including abnormal cotyledon numbers and higher seed weights. We identified AtSMU1 as one of the SMU2-interacting proteins, and *Atsmu1* mutations cause similar developmental phenotypes with higher penetrance than *Atsmu2*. The AtSMU2 and AtSMU1 proteins are localized to the nucleus and highly prevalent in actively dividing tissues. Taken together, our data indicated that the plant SMU-1 and SMU-2 homologues appear to be involved in splicing of specific pre-mRNAs that affect multiple aspects of development.

Pre-mRNA splicing is an essential process where the spliceosome removes introns from pre-mRNAs, and it can lead to more than one splice variant (SV), resulting in the production of different proteins. Alternative splicing has been found to be an important regulatory process in global gene expression, since the splicing pattern of a pre-mRNA can vary in different cell types and at different developmental stages as well as in response to environmental cues (Black, 2003). A model of combinatorial control for pre-mRNA splicing was proposed to explain the apparent complexity of splicing, as the protein complex controlling splice site selection consists of positive- and negative-acting factors (e.g. Ser/Arg-rich [SR] proteins and heterogeneous nuclear ribonucleoproteins [hnRNPs], respectively, that have synergistic and antagonistic interactions; Smith and Valcarcel, 2000; Black, 2003). The balance between splicing factors determines the pattern of pre-mRNA splicing, but tissue-specific regulators appear to be crucial for determining alternative splicing patterns between tissues.

The spliceosome consists of a group of small nuclear RNAs (snRNAs) and proteins that are recruited to pre-mRNAs to remove introns (Jurica and Moore, 2003). Recent proteomic analyses of human spliceosomal complexes (Neubauer et al., 1998; Hartmuth et al., 2002; Jurica et al., 2002; Makarov et al., 2002; Rappsilber et al., 2002; Zhou et al., 2002; Bessonov et al., 2008) revealed nearly 300 putative spliceosomal proteins. Only a fraction of these proteins constitute the catalytic core components for pre-mRNA splicing, while the others are believed to be auxiliary factors. Some of these auxiliary proteins appear to be sequence-specific splicing factors (i.e. recruited to certain sets of pre-mRNAs) or their associated proteins and provide communication links between splicing and other processes in pre-mRNA and mRNA metabolism, such as transcription, capping, and 3′ end formation (Jurica and Moore, 2003). However, the biochemical functions of many such auxiliary factors still remain unknown.

Mechanisms of pre-mRNA splicing in plants are assumed to be similar to those in animals, as the consensus sequences around 5′ and 3′ splice sites and branch sites are similar in plants and animals (Brown

[1] This work was supported by the Department of Energy (grant no. DE–96ER20242 to B.A.L. and grant no. DE–FG02–03ER15438 to R.Y.), the National Science Foundation (grant no. DBI–0077676 to B.A.L. and grant no. IOB–0520008 to R.Y.), the U.S. Department of Agriculture (Cooperative State Research, Education, and Extension Service grant no. 2004–00918 to B.A.L.), and the Agricultural Plant Stress Research Center (grant no. R112001092020080, for partial salary support to C.-S.K.).

[2] Present address: 425-G Henry Mall, Department of Genetics, University of Wisconsin, Madison, WI 53706.

[3] Present address: Department of Plant Biotechnology and Agricultural Plant Stress Research Center, Chonnam National University, Kwangju 500–757, Korea.

* Corresponding author; e-mail larkins@ag.arizona.edu.

The author responsible for distribution of materials integral to the findings presented in this article in accordance with the policy described in the Instructions for Authors (www.plantphysiol.org) is: Brian A. Larkins (larkins@ag.arizona.edu).

[C] Some figures in this article are displayed in color online but in black and white in the print edition.

[W] The online version of this article contains Web-only data.

[OA] Open Access articles can be viewed online without a subscription.

www.plantphysiol.org/cgi/doi/10.1104/pp.109.141705

and Simpson, 1998) and components of animal spliceosomes are conserved in plant genomes (Reddy, 2001). Likewise, precise control of splice site selection during alternative splicing appears to be common and essential in all higher eukaryotes, including plants. The percentage of Arabidopsis (*Arabidopsis thaliana*) genes with alternative splicing is currently estimated to be about 22% (Wang and Brendel, 2006), a value much smaller than is found for humans. But the Arabidopsis genome contains at least 19 genes for SR proteins (Reddy, 2004), almost twice the number of known human SR proteins (Graveley, 2000). SR proteins and some spliceosomal proteins in plants appear to form a functional complex through their physical interactions (Reddy, 2004).

Despite conserved cis-elements and trans-acting factors, the precise function of plant splicing factors is poorly defined. This is partly because an in vitro splicing assay using plant cell extracts is currently unavailable, and a surprisingly small number of mutations in genes encoding putative plant spliceosomal proteins, such as the *supersensitive to ABA and drought1* (*sad1*) and *stabilized1-1* (*sta1-1*) mutants of Arabidopsis (Xiong et al., 2001; Lee et al., 2006), have been reported. *SAD1* and *STA1* encode proteins similar to a human Sm-like snRNP and a human U5 snRNP-associated protein, respectively. Both *sad1* and *sta1-1* manifest altered stress responses as well as morphological defects and reduced growth, indicating that these mutations have pleiotropic effects on plant development. Similarly, developmental defects were obvious in transgenic plants where the production of SR proteins was deregulated. Overexpression of Arabidopsis SR proteins led to pleiotropic effects on developmental programs and influenced splice site selection among SVs encoding the SR proteins themselves as well as other splicing factors (Lopato et al., 1999; Kalyna et al., 2003). More recently, it was found that SR proteins in rice (*Oryza sativa*), when overexpressed, also affect alternative splicing of their own transcripts and those of other SR protein genes (Isshiki et al., 2006).

We isolated an RNA-splicing maize (*Zea mays*) mutant with a variety of phenotypes, including a reduced level of seed storage proteins and defective development of embryos and flowers (Chung et al., 2007). The mutation results from insertion of a transposable element in the first exon of a gene encoding maize ZmSMU2, a homologue of nematode SMU-2 (Spartz et al., 2004), and a human spliceosomal protein (Neubauer et al., 1998; Makarov et al., 2002; Rappsilber et al., 2002; Zhou et al., 2002). Mutations in the nematode *smu-2* gene are associated with altered splicing for *unc-52* pre-mRNA, supporting a role for SMU-2 in pre-mRNA splicing (Spartz et al., 2004). Nevertheless, it is not clear how SMU-2 homologues regulate pre-mRNA splicing. The human SMU-2 homologue does not appear to be a core component of the spliceosome, since it was not uniformly detected in different spliceosomal complexes (Jurica and Moore, 2003; Bessonov et al., 2008). Therefore, it is likely that SMU-2 homologues are auxiliary factors of spliceosomes. Since SMU-2 homologues lack any known RNA-binding domain, these proteins may participate in pre-mRNA splicing by interacting with other spliceosomal proteins.

Based on the sequence homology and pleiotropic nature of the maize mutant, we proposed that *ZmSmu2* plays a role in pre-mRNA splicing. One important prediction from this hypothesis is that one should observe altered splicing of pre-mRNAs in *Zmsmu2* mutants compared with wild-type splicing patterns. Here, we report data supporting this hypothesis. Transcript profiling and reverse transcription (RT)-PCR experiments revealed several potential pre-mRNA targets for ZmSMU2. We further examined the role of other plant SMU-2 homologues using Arabidopsis. We characterized the *AtSMU2* gene and obtained additional evidence supporting the role of SMU-2 homologues in pre-mRNA splicing. We found interactions of ZmSMU2 and AtSMU2 with proteins that imply a link with pre-mRNA splicing and other mRNA metabolic processes. We identified an interaction of AtSMU2 with AtSMU1, the homologue of the nematode SMU-1 protein that was previously shown to interact with SMU-2 (Spartz et al., 2004). Our data suggest that SMU-l and SMU-2 homologues cooperate with other proteins to regulate the splicing of specific pre-mRNAs.

RESULTS

Altered Pre-mRNA Splicing in *Zmsmu2* Mutant Endosperms

To investigate the molecular mechanisms that account for the phenotypes of *Zmsmu2-1* endosperms (Chung et al., 2007), microarray hybridization of RNA from homozygous wild-type and *Zmsmu2-1* endosperms was performed (Supplemental Protocol S1; Supplemental Table S1; Supplemental Fig. S1). Data from this experiment can be summarized as three major observations (for full description, see Supplemental Protocol S1). First, many genes encoding rRNA processing factors and ribosomal proteins are up-regulated in the mutant (Supplemental Figs. S1F and S2), which appears to result from a feedback mechanism that compensates for defective rRNA processing and inefficient protein synthesis in *Zmsmu2* mutant endosperm (Chung et al., 2007). Second, genes involved in the biosynthesis of seed storage proteins are mostly down-regulated in the mutant (Supplemental Figs. S1F and S2), which also explains how the level of seed storage proteins is reduced in the mutant endosperm (Chung et al., 2007). Lastly, it was revealed that many probes with differential gene expression values in the mutant were derived from intronic and alternative exonic sequences (Supplemental Fig. S1E). Furthermore, about 8% of the probes with significantly lower gene expression values in the mutant were

estimated to hybridize with specific SVs, while only 4% of randomly chosen probes appeared to be SV specific (Supplemental Tables S2–S4; Supplemental Protocol S1). These results strongly suggested altered splicing in *Zmsmu2-1* endosperm.

We conducted RT-PCR analysis of selected gene transcripts to compare pre-mRNA splicing in wild-type, *Zmsmu2-1*, and *Zmsmu2-3* endosperms. By an RT-PCR experiment designed to identify SVs, we confirmed at least three pre-mRNAs, SVs of which were differentially accumulated in wild-type and *Zmsmu2-1* endosperm in the microarray experiment. Gene models corresponding to these SVs were manually constructed, based on EST evidence, similarity to conserved protein sequences, and intronic sequence consensus, as described in Supplemental Protocol S1 and Supplemental Figure S1A. These three genes encode TRA2 (an SR-like protein similar to *Drosophila* Transformer2 [Amrein et al., 1988], encoded by GRMZM2G073567 and found on the bacterial artificial chromosome [BAC] clone AC187469.3 at location 124,155–127,755), RSp31B (an SR protein [Gupta et al., 2005], encoded by GRMZM2G021272 and found on the BAC clone AC204569.4 at location 146,139–148,813), and OTUX (an OTU-like protease [Makarova et al., 2000], encoded by GRMZM2G047838 and found on the BAC clone AC232266.1 at location 71,091–75,367). RT-PCR analysis of transcripts for these genes revealed one or more SVs that are preferentially increased or decreased in *Zmsmu2-1* endosperm compared with the wild type (Fig. 1, left panels labeled *Tra2*, *Rsp31b*, and *Otux*), and the relative abundance of these SVs was also found to be affected by the *Zmsmu2-3* mutation (Fig. 1, right panels). For example, the ratio of *Tra2* SV1 to SV3 is higher in *Zmsmu2-1* endosperm than in wild-type or heterozygous siblings (Fig. 1, left panel labeled *Tra2*). Similarly, the ratio of *Rsp31b* SV0 to SV1 is higher in *Zmsmu2-1* than in wild-type or heterozygous siblings (Fig. 1, left panel labeled *Rsp31b*). The altered splicing pattern of *Tra2* and *Rsp31b* pre-mRNAs in *Zmsmu2-3* is very similar to that in *Zmsmu2-1* (Fig. 1). In contrast, the splicing pattern of *Otux* pre-mRNA in *Zmsmu2-3* endosperm is opposite to that in *Zmsmu2-1*: the ratio of *Otux* SV1 to SV2 is lower in *Zmsmu2-3* than in the wild type or a heterozygote, but the ratio is higher in *Zmsmu2-1* than in wild-type or heterozygous sibling endosperms (Fig. 1).

Taken together, the microarray and RT-PCR analyses clearly demonstrated that ZmSMU2 affects alternative splicing of specific pre-mRNAs in developing endosperm, supporting the proposed role of ZmSMU2.

Characterization of *smu2* Mutants in Arabidopsis

To functionally analyze the Arabidopsis homologue of ZmSMU2, we searched the SIGnAL T-DNA Express database (http://signal.salk.edu/cgi-bin/tdnaexpress; Alonso et al., 2003) for mutants with T-DNA insertions in the *AtSMU2* gene (At2g26460). Two putative mutants were identified and designated *Atsmu2-1* and *Atsmu2-2*, respectively. Analysis of the T-DNA-flanking sequences revealed that the *Atsmu2-1* T-DNA was in the eighth exon of the gene (Fig. 2A). In *Atsmu2-2*, a T-DNA insert was confirmed in the sixth intron of the gene (Fig. 2A). To investigate the effect of these mutations on *AtSMU2* gene expression, RT-PCR analysis of RNA from seedlings was performed using different combinations of primers (for the locations of the primers, see Fig. 2A). The *Atsmu2-1* (Fig. 2B, lane 2) and *Atsmu2-2* (Fig. 2B, lane 3) homozygous seedlings did not show significant differences in RNA levels corresponding to the 5′ portion of the *AtSMU2* coding sequence [Fig. 2B, *AtSMU2* (1–2)] as compared with wild-type seedlings (Fig. 2B, lane 1). However, when primers flanking the T-DNA insertion sites were used, *SMU2* transcripts were not detected in the mutants [Fig. 2B, *AtSMU2* (3–4)], indicating that the T-DNA insertions disrupted proper transcription, pre-mRNA splicing, or RNA stability. Thus, *Atsmu2-1* and *Atsmu2-2* homozygous mutant plants are unlikely to produce a wild-type AtSMU2 protein. However, RT-PCR analysis

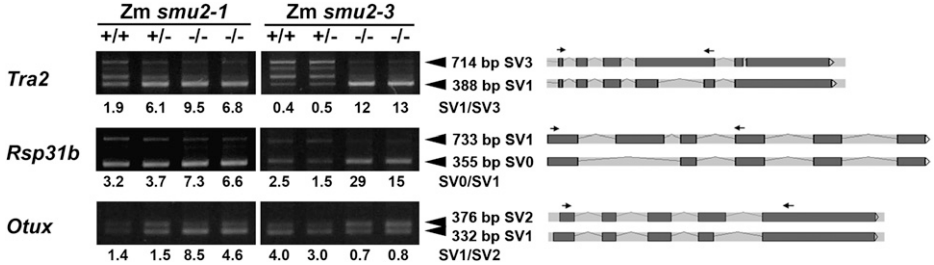

Figure 1. Altered RNA splicing in *Zmsmu2-1* and *Zmsmu2-3* endosperm. Heterozygous (*smu2-1*/+ or *smu2-3*/+) plants were self-pollinated, and kernels were dissected into embryo and endosperm tissues at 16 d after pollination. Embryo DNA was used to genotype the *Zmsmu2* locus, and RNA was extracted from homozygous wild-type, heterozygous, and homozygous mutant endosperms and used for semiquantitative RT-PCR. +/+, Endosperm with a homozygous wild-type embryo; +/−, endosperm with a heterozygous embryo; −/−, endosperm with a homozygous *smu2-1* mutant embryo. Arrowheads indicate SVs with different band intensities between the wild type and mutants. Pre-mRNA splicing patterns of SVs are shown at right, with RT-PCR primers indicated by arrows. Ratios of differentially accumulated SVs are shown below the panels.

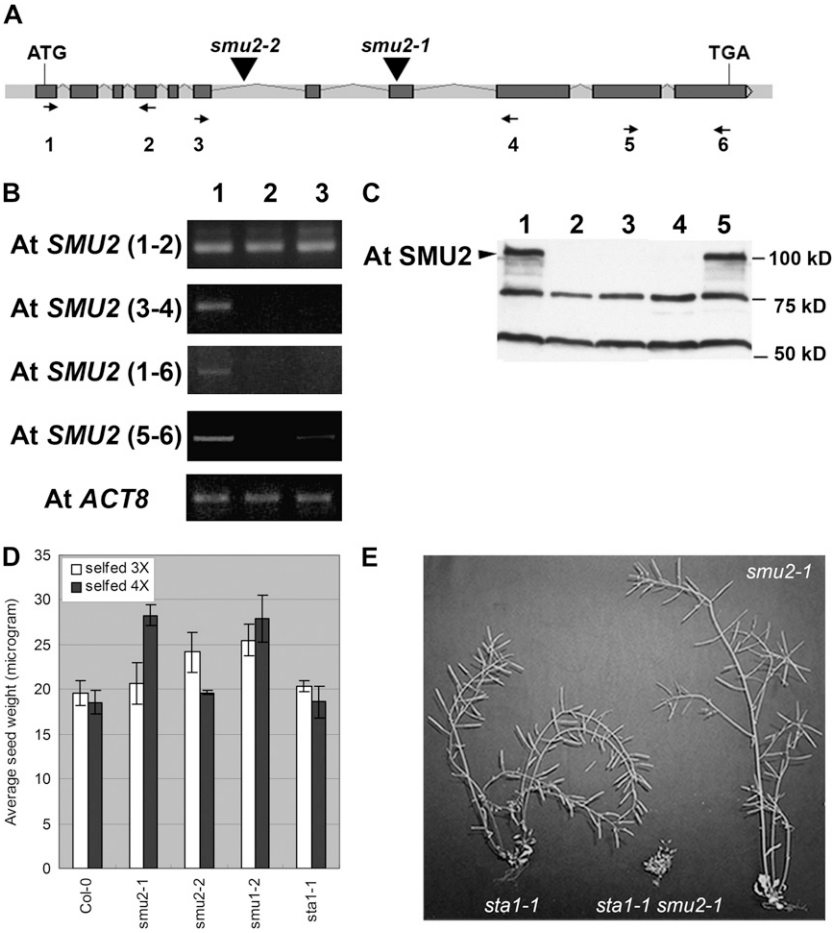

Figure 2. A, Structure of the *AtSMU2* gene. Dark gray boxes and light gray bars between the boxes represent exons and introns, respectively. Triangles indicate T-DNA insertion sites in the *Atsmu2-1* and *Atsmu2-2* mutants. B, RT-PCR analysis of *AtSMU2* transcripts. Four pairs of primers were used for amplifying different regions of the *AtSMU2* mRNA sequence prepared from wild-type 14-DAG Col-0 (lane 1), *smu2-1* (lane 2), and *smu2-2* (lane 3) seedlings. Numbers in parentheses indicate the primers used for RT-PCR, and their positions are shown as arrows in A. *AtACT8* transcript encoding an actin was used as an internal control. C, Immunoblot analysis of AtSMU2 using protein extracts from four 7-DAG Col-0 (lane 1), *smu2-1* (lane 2), *smu2-2* (lane 3), *smu1-2* (lane 4), and *sta1-1* (lane 5) seedlings as described by Chung et al. (2007). The arrowhead indicates the AtSMU2 protein. D, Phenotypic analyses of various mutants. Homozygous mutant plants (*smu2-1*, *smu2-2*, *smu1-2*, and *sta1-1*) were identified among segregating populations and were subsequently self-pollinated two or three times. Phenotypic analysis was conducted as described in "Materials and Methods." E, Dry *sta1-1* (left), *smu2-1 sta1-1* (middle), and *smu2-1* (right) plants.

using primers downstream to the T-DNA insertion sites indicated a low level of detectable RNA in the *Atsmu2-2* mutant plants [Fig. 2B, *AtSMU2* (5–6)]. This suggests that the T-DNA insertion in *Atsmu2-2* may create a downstream, cryptic transcription start site that can lead to the production of a partial *AtSMU2* mRNA.

To determine whether the mutant plants lacked a full-length AtSMU2 protein, an immunoblot analysis of extracts from wild-type and *Atsmu2-1* and *Atsmu2-2* mutant plants was conducted. We previously reported that an AtSMU2 protein with a glutathione-*S*-transferase (GST) tag showed strong cross-reaction with an antiserum prepared against ZmSMU2 (Chung et al., 2007). Of the three prominent bands detected in wild-type Arabidopsis seedlings, the largest band corresponding to a 100-kD protein was absent in the mutant extracts (Fig. 2C), indicating that it corresponds to the AtSMU2 protein. Furthermore, this result showed that *Atsmu2-1* and *Atsmu2-2* mutant plants do not produce a full-length AtSMU2 protein, suggesting that the two alleles are null for AtSMU2 function.

In order to understand the function of the *AtSMU2* gene during development, we analyzed the phenotypes of the *smu2-1* and *smu2-2* plants. The first generation homozygous mutant seedlings appeared to grow slower than wild-type seedlings, although their overall architecture was indistinguishable from that of wild-type plants (data not shown). On the other hand, we observed the appearance of abnormal phenotypes after further selfing of the mutant alleles. For example, the weight of seeds produced in the F4 populations (self-pollinated three times) of the *smu2-1* plants was not significantly different from that of the wild-type seeds, while that of the F5 populations (self-pollinated four times) was considerably greater (Fig. 2D). Homozygous *smu2-2* F4 seeds were significantly heavier than wild-type seeds (Fig. 2D), although the F5 seeds were similar in weight to wild-type seeds (Fig. 2D). In addition, *smu2-1* and *smu2-2* plants produced a low frequency of abnormal seedlings with one, three, or more cotyledons in some F3 and F4 populations. For example, 0.4% of *smu2-1* F4 seedlings ($n = 744$) showed abnormal cotyledon number as compared with no abnormal seedlings ($n = 1{,}443$) observed from wild-type ecotype Columbia (Col-0) plants (Table I). However, these phenotypes were not completely penetrant and varied depending on the individual parental plants tested (effectively preventing a genetic complementation of the mutant). Taken together, the genetic evidence indicates that the *AtSMU2* gene may play a

Table I. *Arabidopsis mutant phenotypes in seedling development*

Values are presented as means ± SD.

Genotype	Generation	Abnormal Cotyledon Number[a]	Germination Failure or Arrested Growth[a]
		%	%
Col-0	F4	0 ± 0	0.2 ± 0.3
	F5	0 ± 0	0.1 ± 0.2
smu2-1	F4	0.4 ± 0.5	0.8 ± 1.0
	F5	0 ± 0	0.1 ± 0.3
smu2-2	F4	0.3 ± 0.4	0.6 ± 0.4
	F5	0.2 ± 0.3	0.8 ± 0.7
smu1-2	F4	45.8 ± 4.8	13.9 ± 8.6
	F5	10.0 ± 2.0	10.5 ± 8.8
SMU1^{Bar}/_; smu1-2	T2	0.4 ± 0.5	0 ± 0
SMU1-GFP^{Bar}/_; smu1-2	T2	2.3 ± 1.4	0.3 ± 0.8
sta1-1	F4	2.8 ± 1.0	0.5 ± 0.7
	F5	0.3 ± 0.3	0.2 ± 0.3

[a]Phenotypes were scored as described in "Materials and Methods."

subtle role in seed development under certain conditions.

Genetic Interaction between *Atsmu2* and *sta1*

To investigate any role for *SMU2* in pre-mRNA splicing in Arabidopsis, we created double-mutant combinations between *Atsmu2* alleles and a mutation in the *STA1* gene, which encodes a conserved protein with high similarity to the human U5 snRNP-associated 102-kD protein and the yeast proteins PRP1p and Prp6p (Lee et al., 2006). The *sta1-1* mutant used here is likely a partial loss-of-function allele, because it contains a two-codon deletion in the coding region. Homozygous *sta1-1* plants exhibit mild developmental defects, including delayed growth and serrated leaf margins (Lee et al., 2006). We observed that although the size of the mutant plants was typically smaller than that of wild-type plants, they often showed more shoots per plant and produced a comparable number of seeds as wild-type plants (Fig. 2E). The weight of the seeds obtained from *sta1-1* mutants was not significantly different from that of wild-type plants (Fig. 2D). The *sta1-1* mutant plants also showed several additional phenotypes, including an abnormal number of cotyledons (n = 984; Table I).

No double mutants were identified among 114 F2 plants analyzed from a cross of homozygous *Atsmu2-1* and *sta1-1* plants. Further genotyping of 52 F3 plants that were homozygous for *smu2-1* and segregating for *sta1-1* and *STA1* resulted in the identification of four *smu2-1 sta1-1* double mutant plants, three of which produced three cotyledons while one produced two cotyledons of different sizes. Three of the double mutant plants died before flowering, but one with three cotyledons developed numerous small leaves and short inflorescences bearing only one or two short siliques (Fig. 2E) with one or two seeds per silique. None of the 15 seeds obtained from this plant germinated. Similar results were obtained using the *smu2-2* allele in combination with *sta1-1*. No double mutant plants were obtained from F2 plants segregating for *smu2-2* and *sta1-1*, while three double mutants were identified from F3 populations. All three *smu2-2 sta1-1* double mutant seedlings ceased to grow at the cotyledon stage or before flowering. Plants that are either homozygous for *sta1-1* and heterozygous for *smu2-2* or heterozygous for *sta1*-1 and homozygous for *smu2-2* produced partially filled siliques, suggesting that most of the double mutants are aborted in early seed development. Thus, compared with the single mutant parental plants (Fig. 2E), the *smu2 sta1* double mutant plants exhibited a more severe set of developmental defects. Together with the observation that *smu2* single mutants are phenotypically distinct from *sta1-1*, this genetic interaction indicated that *AtSMU2* has at least some nonoverlapping functions with *STA1*.

The *Atsmu2* Mutations Cause Pre-mRNA Splicing Defects

To investigate whether AtSMU2 functions in pre-mRNA splicing, we analyzed *Atsmu2* mutant seedlings for genes previously known to produce SVs. Using RT-PCR, we detected three previously described SVs (mRNA1, -2, and -3) for the At1g09140 (*AtSRp30*) gene (Lopato et al., 1999) in both wild-type and mutant plants (Fig. 3). However, the ratio of mRNA1 to mRNA3 was higher in the two mutants than in wild-type seedlings (Fig. 3). Furthermore, an additional SV candidate was detected specifically in the mutant seedlings (Fig. 3, asterisks). Analysis of other genes known to undergo alternative splicing, however, did not indicate any differential accumulation of their SVs in the mutant seedlings (data not

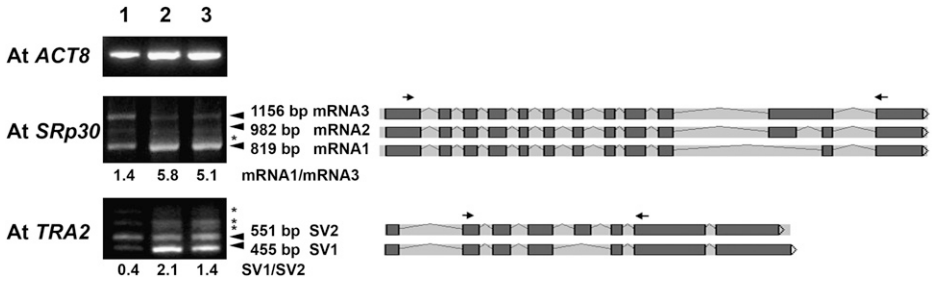

Figure 3. RT-PCR detection of SVs in *Atsmu2-1* and *Atsmu2-2*. RT-PCR was performed using total RNA from 14-DAG Col-0 (lane 1), *smu2-1* (lane 2), and *smu2-2* (lane 3) seedlings. Arrowheads indicate the positions of known SVs of At1g09140 (*AtSRp30*) and At1g07350 (*AtTRA2*), while asterisks correspond to putative SVs first observed here. Pre-mRNA splicing patterns are shown on the right side, with dark gray boxes and light gray bars between the boxes representing exons and introns, respectively. Arrows depict primers used in each reaction. Ratios of differentially accumulated SVs are shown below the panels.

shown), suggesting that only a certain number of alternative splicing events were affected by the *Atsmu2-1* mutation.

Interestingly, *AtSRp30* encodes a protein showing sequence similarity to ZmRSp31B. Based on this, we speculated that *Zmsmu2*-dependent alternative splicing events might be evolutionarily conserved if they are functionally significant for the two species. A search of the Arabidopsis protein sequence database identified At5g04250 (OTUX-like) and At1g07350 (AtTRA2) as putative homologues of OTUX and TRA2, respectively. Analysis of the *AtTRA2* mRNA from wild-type plants indicated the presence of four SVs (Fig. 3), two of which (SV1 and -2) were previously annotated in The Arabidopsis Information Resource (http://www.arabidopsis.org). As shown in Figure 3, the accumulation of SV1 relative to SV2 was elevated in *Atsmu2-1* and *Atsmu2-2* seedlings as compared with wild-type seedlings. These data indicate that the *Atsmu2* mutations affect alternative splicing of specific pre-mRNAs. Thus, AtSMU2 may function as a pre-mRNA splicing factor, similar to the role played by its homologues in nematodes and maize.

Expression of *AtSMU2* during Development

Involvement of AtSMU2 in pre-mRNA splicing would suggest that the protein is localized to the nucleus. To test this, we generated transgenic Arabidopsis plants that produced an AtSMU2-GFP fusion product under the control of a modified cauliflower mosaic virus 35S gene promoter/enhancer sequence. As shown in Figure 4C, the AtSMU2-GFP fusion protein was localized exclusively to the root cell nuclei. In contrast, a nonconjugated GFP protein control was detected in both cytoplasm and the nucleus (Fig. 4A) and a GUS-GFP fusion protein control was detected exclusively in the cytoplasm (Fig. 4B). Therefore, the nuclear localization of AtSMU2 corresponds to its putative function in pre-mRNA splicing.

Immunoblot analysis of ZmSMU2 in various maize tissues indicated the highest levels of expression in rapidly developing tissues or organs, such as the developing endosperm, embryo, shoot apex, and flower (Chung et al., 2007). To identify the highest levels of protein accumulation for AtSMU2 during development, we extracted proteins from various Arabidopsis organs and performed immunoblot analysis using anti-ZmSMU2 antibodies. As shown in Figure 5, the highest levels of AtSMU2 protein was detected in seedlings at 7 d after germination (DAG; lane 1), young flowers before anthesis (lane 6), and developing siliques less than 5 mm in length (lane 8). Lower levels of AtSMU2 accumulation were detected in roots (lane 2), expanding cauline leaves (lane 4), open flowers (lane 7), and dry seeds (lane 9), while the inflorescence (lane 5) contained only a trace amount of the protein, which was only detectable when the immunoblot was overexposed. No protein was detected in senescing rosette leaves (lane 3). Thus, the AtSMU2 protein, like ZmSMU2 (Chung et al., 2007), appears to be present throughout the plant, although

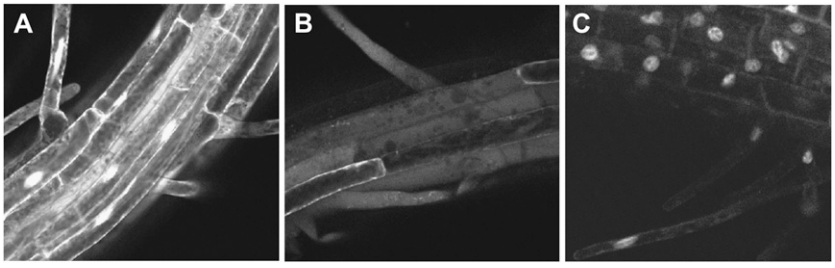

Figure 4. Subcellular localization of AtSMU2 fusion protein. A, Arabidopsis root cells overexpressing GFP showed a diffused localization pattern in the cytosol and the nuclei. B, GUS-GFP in Arabidopsis root cells was exclusively localized in the cytosol. C, Arabidopsis root cells overexpressing AtSMU2-GFP exhibited nucleus-specific localization.

Figure 5. Immunoblot analysis of AtSMU2 showing accumulation of AtSMU2 protein in various organs and structures of Arabidopsis. Each lane contained approximately 10 μg of proteins from reproductive and vegetative organs of Col-0 plants. Lane 1, Seedlings at 7 DAG; lane 2, roots of 30-DAG plants; lane 3, senescing rosette leaves; lane 4, young cauline leaves; lane 5, inflorescence; lane 6, immature flowers; lane 7, open flowers; lane 8, developing siliques (less than 5 mm in length); lane 9, dry seeds.

its abundance varied, with the highest level of accumulation in mitotically active tissues and organs.

ZmSMU2 and AtSMU2 Interact with AtSMU1

To gain additional insight into the molecular functions of plant SMU-2 homologues, we used the yeast two-hybrid (Y2H) system to identify proteins that interacted with ZmSMU2. Transformants containing a GAL4 binding domain fused to a full-length ZmSMU2 protein exhibited self-activation (Fig. 6A). Removal of the N terminus (residues 1–374, construct IV) or C terminus (residues 360–565, construct V) substantially reduced the self-activation (Fig. 6A), allowing us to create a fusion protein bait to screen two maize libraries and one Arabidopsis library. In a screen of a maize endosperm library using construct IV as a bait, six colonies were obtained, all of which encoded a full-length histone H4 cDNA. To expand the repertoire of ZmSMU2-interacting proteins, we used construct V as a bait to screen a cDNA library prepared from young maize ears. This analysis resulted in the identification of six ZmSMU2-interacting proteins represented by 38 clones (Table II, clone identifiers starting with Zm), including an SMU-1-like protein containing WD40 repeats (Spartz et al., 2004). Three additional putative ZmSMU2-interacting proteins were identified from a screen of an Arabidopsis library of 3-DAG seedlings using construct V as a bait (Table II, clone identifiers starting with At).

We primarily focused on the interaction of AtSMU2 and ZmSMU2 with the SMU-1-like protein, because previous findings indicated that SMU-1 and SMU-2 homologues are likely partners in the formation of a functional spliceosome complex. The *Caenorhabditis elegans* SMU-1, which also contains WD40 repeat motifs, interacts with SMU-2 (Spartz et al., 2004), and the human SMU1 and SMU2 proteins were found within human spliceosomal complexes (Jurica and Moore, 2003). Therefore, we used in vitro pull-down assays to confirm the Y2H interactions indicated above. As shown in Figure 6B, the GST-AtSMU2 and GST-ZmSMU2 recombinant proteins when used as baits were capable of pulling down His-tagged AtSMU2 and histone H4 proteins in vitro. No interaction was detected when GST alone was used to pull down the

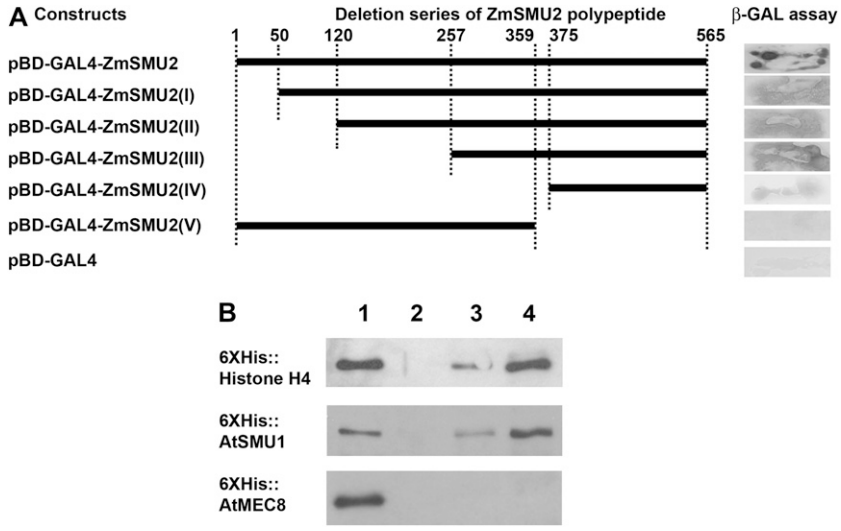

Figure 6. Interactions of ZmSMU2 and AtSMU2 with other proteins. A, Y2H bait constructs were tested for self-activation and the corresponding β-GAL assays. A construct containing the full-length ZmSMU2 protein (pBD-GAL4-ZmSMU2; top) exhibited strong self-activation of the β-GAL reporter gene when introduced into Y190 cells. N-terminal deletions of ZmSMU2 (bait constructs I–IV) also showed self-activation, albeit at lower levels than for the full-length protein. Only a C-terminal deletion (bait construct V) and a negative control (pBD-GAL4; bottom) did not activate the reporter gene. Black bars represent the ZmSMU2 polypeptides. Numbers above the bars indicate amino acid residues corresponding to the full-length ZmSMU2 polypeptide. B, Confirmation of Y2H screen by in vitro pull-down assay using GST or GST fusion protein as a bait. GST (lane 2), GST-AtSMU2 (lane 3), or GST-ZmSMU2 (lane 4) bound to glutathione-agarose beads was used to pull down 6XHis-histone H4, 6XHis-AtSMU1, or 6XHis-AtMEC8. Lane 1, Ten percent input; lanes 2, 3, and 4, 30% pull-down by GST, GST-AtSMU2, and GST-ZmSMU2, respectively.

Table II. *Summary of a Y2H screen for proteins interacting with ZmSMU2*

Clone Identifier	TopBLASTN[a]	Percentage Identity[b]	Predicted Protein[c]
Zm6-1	DV495718.1	100	Rasputin-like protein (Pazman et al., 2000)
Zm8-1	BU051217.1	98	Histone H4
Zm17-3	DN226990.1	97	SMU-1-like protein (Spike et al., 2001)
Zm31-7	DN218694.1	96	VOZ-like protein (Mitsuda et al., 2004)
Zm33-8	CA404370.1	97	EF-1β
Zm59-20	DT654009.1	96	Glycerol kinase-like protein
At1-1	NM_103009.3	97	$TAF_{II}250$-like HAF01, partial (Bertrand et al., 2005)
At2-3	NM_118947.2	98	TPR protein, partial
At3-3	NM_117736.2	99	DUF751-containing protein

[a]GenBank accession numbers with the highest nucleotide sequence similarity to the Y2H clone shown in the left column. [b]The percentage of nucleotide sequence identity based on BLASTN analysis. [c]Based on the BLASTX result for the TopBLASTN sequences.

target proteins (Fig. 6B, lane 2). In addition, a His-tagged AtMEC8 used as a control also did not show interaction with the GST-AtSMU2 and GST-ZmSMU2 proteins. The AtMEC8 protein is an Arabidopsis counterpart of the nematode MEC-8 that contains two RNA recognition motifs and has been shown to regulate alternative splicing of the unc-52 transcripts (Lundquist et al., 1996). Taken together, these data indicate that the AtSMU2 and ZmSMU2 proteins interact with SMU1, a highly conserved component of the eukaryotic spliceosome.

Expression of AtSMU1 during Development

To examine the expression of *AtSMU1* during development, we generated a GFP fusion construct under the control of the endogenous promoter (*AtSMU1-GFP*^{Kan}) and introduced it into Arabidopsis plants. The AtSMU1-GFP fusion protein was detected mainly in actively dividing cells, such as the newly emerged leaf and the root tip of seedlings (Fig. 7, A–C). A close examination of these structures using confocal microscopy revealed that the fusion protein was likely nucleus localized (Fig. 7, D and E). This was further confirmed in the root hair cells using colocalization of 4′,6-diamino-phenylindole (DAPI) and GFP signals (Fig. 7, F–H). GFP expression was detected during embryogenesis including the heart stage of embryo development (Fig. 7, L–N). The AtSMU1-GFP fusion product was also detected in the nuclei of all cell types within the female gametophyte, including egg cell, central cell, synergid cells (Fig. 7J), and the antipodal cells (data not shown). Within the mature pollen, GFP signal was localized to both vegetative and generative nuclei (Fig. 7K). These results indicate that the subcellular localization and distribution of AtSMU1 protein are similar to those of AtSMU2.

Molecular and Genetic Characterization of *AtSMU1*

Identification of ZmSMU1 and AtSMU1 proteins as interacting partners for ZmSMU2 and AtSMU2 prompted us to investigate the phenotype of *smu1* loss-of-function alleles. Like *AtSMU2*, *SMU1* appeared to be a single-copy gene in the Arabidopsis genome. We identified three putative T-DNA insertional mutant alleles in the *AtSMU1* gene (At1g73720) and designated them *smu1-1* (SALK_123852), *smu1-2* (SALK_051163), and *smu1-3* (SAIL_95_E04). Sequencing of the genomic DNA flanking these insertions revealed that the T-DNAs in the *smu1-1* and *smu1-2* alleles were located within exon 11 and intron 15, respectively (Fig. 8A). By contrast, the *smu1-3* allele contained a T-DNA insertion in the promoter region. Analysis of the individual segregants from selfing populations of heterozygous *smu1-1*/+, *smu1-2*/+, or *smu1-3*/+ plants indicated that *AtSMU1* may be required for plant viability. Homozygous *smu1-1* seedlings could not be maintained under normal growth conditions, as they were extremely dwarfed (1–5 mm in diameter), developed many small leaves, and did not produce any flowers (data not shown). This suggested that in comparison with the *smu1-2* allele (see below), *smu1-1* is likely a complete loss-of-function allele. On the other hand, homozygous *smu1-2* plants were generally more viable and reached the flowering stage despite exhibiting a syndrome of developmental abnormalities including (but not limited to) abnormal cotyledon number (Table I; Fig. 8B), increased seed weight (Fig. 2D), abnormal flower positions (node spacing; Fig. 8B), and seed germination defects (Table I). However, some of these phenotypes were associated with a reduced penetrance that varied significantly from generation to generation (Table I). The reduced severity of the phenotypes observed in *smu1-2* plants was consistent with the intronic T-DNA insertion site in this allele, indicating that *smu1-2* is a weaker allele than *smu1-1*. Finally, in contrast to the *smu1-1* and *smu1-2* alleles, *smu1-3* did not exhibit any phenotypic changes, indicating that the upstream T-DNA insertion in this allele did not affect *AtSMU1* gene expression.

To see if the *smu1-2* phenotypes are caused by T-DNA insertion in the corresponding gene, we per-

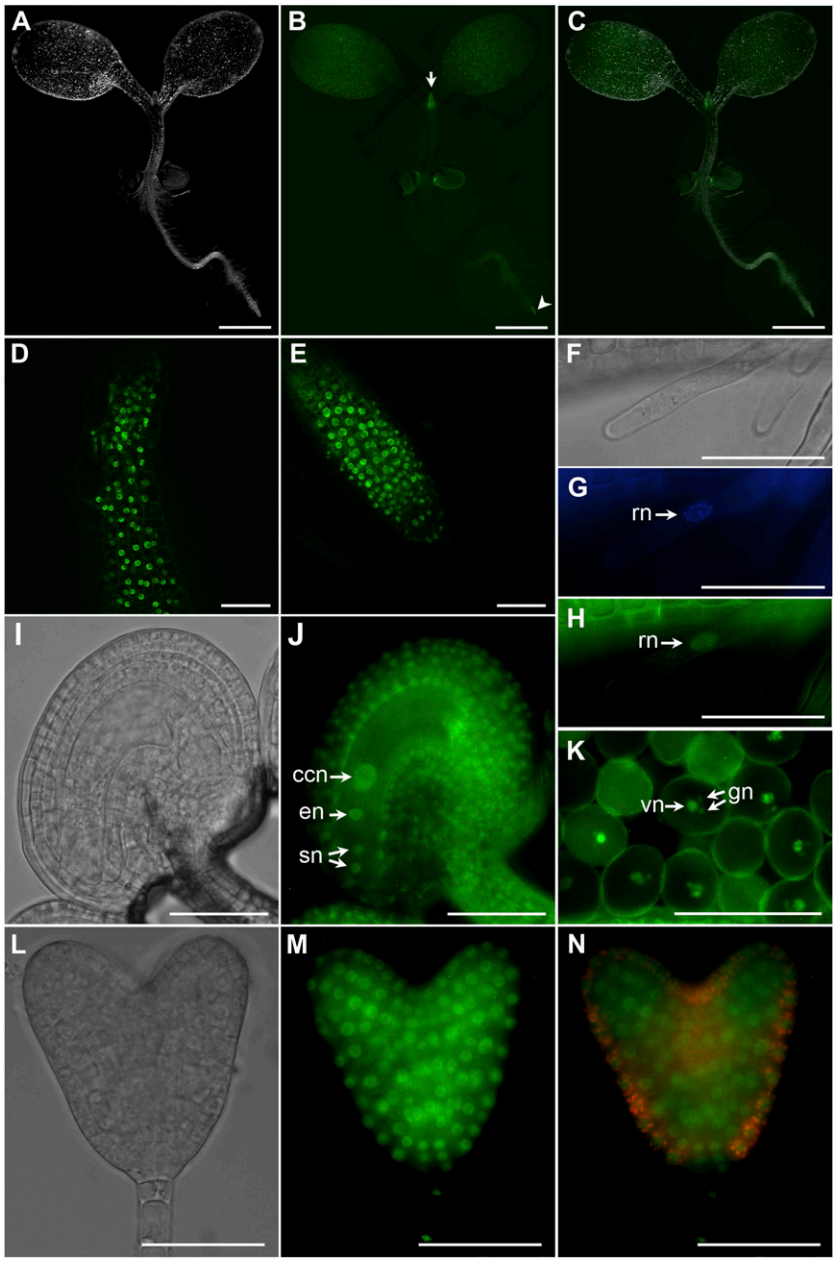

Figure 7. Expression of *SMU1-GFP*^{kan} during plant development. A to C, Dark-field, epifluorescence GFP, and merged images of a kanamycin-resistant seedling. The arrow points to a newly emerged leaf. The arrowhead points to the root tip. D, Confocal image of the area indicated by the arrow in B. E, Confocal image of the area indicated by the arrowhead in B. F to H, Bright-field, epifluorescence DAPI, and GFP images of a root hair. I and J, Bright-field and epifluorescence GFP images of a flower stage 13 ovule. K, Epifluorescence GFP image of mature pollen. L to N, Bright-field, epifluorescence GFP, and fluorescein isothiocyanate images of a heart-stage embryo. ccn, Central cell nucleus; en, egg cell nucleus; gn, generative nuclei; rn, root hair nucleus; sn, synergid nuclei; vn, vegetative nucleus. Bars = 1 mm in A to C and 50 μm in D to N.

formed complementation of the mutant with the wild-type *AtSMU1* gene. In addition to construct *AtSMU1-GFP*^{Kan}, we also generated construct *AtSMU1-GFP*^{Bar} and *AtSMU1*^{Bar} and transformed *smu1-2* heterozygous plants. For construct *AtSMU1-GFP*^{Bar}, we obtained 41 T1 transformants, and five of them were homozygous for the *smu1-2* mutant allele. The GFP expression pattern of *AtSMU1-GFP*^{Bar} was similar to that of *AtSMU1-GFP*^{Kan}. For construct *AtSMU1*^{Bar}, we obtained 21 T1 transformants, and seven of them were homozygous for the *smu1-2* mutant allele. The T1 transformants homozygous for *smu1-2* germinated and grew normally, developed two cotyledons, and showed normal node spacing in the inflorescence. The T2 populations segregating for the transgenes displayed close to normal germination rates and cotyledon morphology (Table I). This phenotypic rescue by the transgenes clearly demonstrates that the *Atsmu1-2* phenotypes are caused by the T-DNA insertion in the *AtSMU1* gene.

To confirm that the T-DNA insertion in *smu1-2* affected the expression of *AtSMU1*, we used RT-PCR to amplify *AtSMU1* RNA in wild-type and mutant plants. As shown in Figure 8C, the RT-PCR product obtained with *AtSMU1*-specific primers indicated that the transcript in *smu1-2* seedlings lacked the 3′ terminal region of the coding sequence. The RT-PCR product with another pair of *AtSMU1*-specific primers [Fig. 8C, *AtSMU1* (3–4)] showed that the mutant seedlings accumulated reduced levels of *AtSMU1*

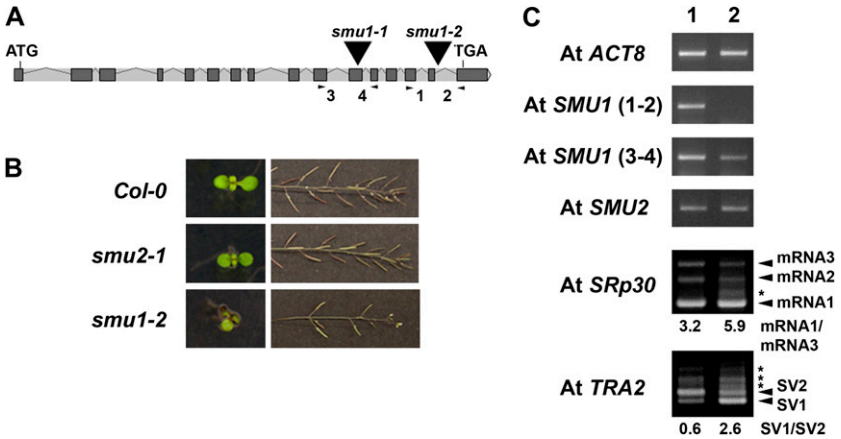

Figure 8. Analysis of *Atsmu1* mutant alleles. A, Structure of the *AtSMU1* gene and the T-DNA insertions in the *Atsmu1-1* and *Atsmu1-2* mutants (triangles). B, Phenotypes of Col-0 wild-type, *Atsmu2-1* (F4), and *Atsmu1-2* (F3) plants. Seedlings of *smu1-2* at 7 DAG often showed an abnormal number of cotyledons (left panels; see Table I) and arrangement of flowers/siliques in the primary inflorescence (right panels). C, RT-PCR comparison of *AtSMU2*, *AtSMU1*, *AtSRp30*, and *AtTRA2* transcripts in Col-0 and *smu1-2*. Two pairs of primers were used to amplify different regions of the *AtSMU1* cDNA prepared from 14-DAG seedlings of Col-0 (lane 1) and *smu1-2* (lane 2) plants. Numbers in parentheses indicate the primers used for the RT-PCR; the positions of the primers are shown as arrowheads in A. Arrowheads indicate the positions of known SVs of *SRp30* and *TRA2*, while asterisks correspond to the potentially novel SVs. Ratios of differentially accumulated SVs are shown below the panels. [See online article for color version of this figure.]

transcript compared with the wild type. The *smu1-2* mutation did not appear to affect *AtSMU2* mRNA levels (Fig. 8C, *AtSMU2*). Nevertheless, AtSMU2 protein was not detected in *smu1-2* mutant extract (Fig. 2C, lane 4), whereas its level in the *sta1-1* mutant was comparable to that of the wild type (Fig. 2C, lanes 1 and 5). These data indicate that the expression of *AtSMU1* is required for proper accumulation of the AtSMU2 protein in the cell.

Protein interaction studies (see above) indicated that AtSMU1 may function in pre-mRNA splicing in a complex with AtSMU2. Therefore, we predicted that the *smu1-2* mutant would manifest altered splicing of *AtTRA2* and *SRp30* pre-mRNAs, as was observed in *Atsmu2-1* and *Atsmu2-2* mutant plants. As shown in Figure 8C, the relative abundance of *AtTRA2* and *SRp30* SVs in *smu1-2* resembled those seen in *smu2-1* and *smu2-2* mutant plants (Fig. 3). These data indicate that *AtSMU1* and *AtSMU2* are involved in the alternative splicing of common pre-mRNAs.

DISCUSSION

We hypothesized that ZmSMU2 is a pre-mRNA splicing factor (Chung et al., 2007), and data presented in this paper provide additional evidence supporting this hypothesis. We found an evolutionarily conserved protein interaction between SMU-1 and SMU-2 homologues (Fig. 6) and nuclear localization of AtSMU2-GFP (Fig. 4) and AtSMU1-GFP (Fig. 7). Intriguingly, *Zmsmu2*, *Atsmu2*, and *Atsmu1* mutants showed an altered pattern of pre-mRNA splicing (Figs. 1, 3, and 8). It is known that overexpression of splicing regulators in plants and animals, including SR proteins, often leads to altered splicing of their own RNAs and that of other splicing regulators (Bell et al., 1991; Jumaa and Nielsen, 1997; Lopato et al., 1999; Kalyna et al., 2003; Isshiki et al., 2006). In this regard, the altered splicing patterns of *Rsp31b* and *Tra2* in *Zmsmu2-1* and *Zmsmu2-3* endosperm (Fig. 1) are particularly interesting, because these genes encode an SR and an SR-related protein, respectively. The altered splicing that occurs when splicing regulators are overexpressed may be due to an autoregulatory mechanism of the splicing regulatory network. This mechanism, although not understood, is being actively investigated (Wollerton et al., 2004; Kumar and Lopez, 2005). Altered splicing of *Tra2* and *Rsp31b* pre-mRNAs in *Zmsmu2-1* could also be a secondary consequence of the *Zmsmu2-1* and *Zmsmu2-3* mutations (i.e. *Tra2* and *Rsp31b* might not normally be primary targets of the ZmSMU2 protein). Consistent with this, the microarray data indicated that expression of genes encoding splicing regulators was down- or up-regulated in *Zmsmu2-1* endosperm (Supplemental Table S1). Among these putative splicing regulators are an SRp75-like protein, a KH domain-containing protein, a TIA-1-like oligouridylate-binding protein, and a hnRNP A2/B1-like protein (Supplemental Table S1).

In contrast to SVs for *Tra2* and *Rsp31b* genes, *Zmsmu2-1* and *Zmsmu2-3* endosperms showed opposite effects on the splicing pattern in *Otux* pre-mRNA (Fig. 1). Importantly, the ZmSMU2 protein level is higher in *smu2-1* mutant endosperm than in its wild-type sibling, while it is lower in *smu2-3* than in the corresponding wild type (Chung et al., 2007). Therefore, if the action of ZmSMU2 as a splicing factor follows a model of combinatorial control for pre-

mRNA splicing (Smith and Valcarcel, 2000; Black, 2003), *Otux* pre-mRNA may represent a true target of the ZmSMU2 splicing factor, since its splicing depends on the concentration of ZmSMU2 protein.

Our genetic data also indicate that *AtSMU1* and *AtSMU2* function in a similar pathway to control pre-mRNA splicing in Arabidopsis. Similar to *Zmsmu2* mutants, *Atsmu2-1*, *Atsmu2-2*, and *Atsmu1-2* showed alterations in *AtTRA2* and *SRp30* splicing patterns (Figs. 3 and 8C). Consistent with the proposed role of the plant SMU-2 homologues in pre-mRNA splicing, the *Zmsmu2*, *Atsmu2*, and *Atsmu1* mutants are all pleiotropic. The *Zmsmu2-1* mutant embryos often produce twin shoots and roots (Chung et al., 2007). Similarly, the *Atsmu1-2* mutation is associated with an abnormal number of cotyledons and irregular inflorescence architecture (Fig. 8), indicating an abnormal meristematic function. Multiple developmental phenotypes are also associated with *Atsmu2* mutations, albeit low in penetrance. In addition, the *Atsmu1* and *Atsmu2* mutants showed similar phenotypes, including increased seed weight (Fig. 2D) and abnormal cotyledon number (Table I). Increased seed weight was not associated with a mutation in the *STA1* gene, which presumably encodes a core spliceosomal protein, although *sta1-1* mutant seedlings have similar defects in germination and cotyledon development. Furthermore, *Atsmu2 sta1* double mutants showed very severe developmental defects (Fig. 2E), suggesting that the targets of *STA1* may not overlap with those of the *AtSMU2* gene in the main.

It remains to be seen what pre-mRNA targets for plant SMU-2 homologues are responsible for the developmental phenotypes of *Zmsmu* and *Atsmu* mutants, although our microarray analysis of *Zmsmu2* endosperm suggested extensive changes in the expression of genes controlling the biosynthesis and perception of plant hormones (Supplemental Table S1). Notably, an abnormal number of cotyledons and twin embryos were also caused by ectopic expression of *AtRSZ33*, which encodes an Arabidopsis SR protein (Kalyna et al., 2003). Spartz et al. (2004) proposed that SMU-2 may act similarly to SR-related proteins, which also lack RNA-binding motifs. In fact, we observed several features shared by ZmSMU2 and SR proteins. First, *Zmsmu2* mutations are associated with altered splicing patterns in multiple pre-mRNAs, including those encoding SR proteins (Fig. 1). This effect has been observed in plant and animal cells overexpressing SR proteins (Mizzen et al., 1996; Jumaa and Nielsen, 1997; Lopato et al., 1999; Kalyna et al., 2003; Kumar and Lopez, 2005). In addition, expression of Arabidopsis SR protein genes appeared to be tissue specific and particularly high in pollen and in actively dividing cells (Lopato et al., 1999, 2002; Kalyna et al., 2003). This pattern of expression is very similar to that observed in *AtSMU2* and *AtSMU1* genes (Figs. 5 and 7).

Our study of protein interactions with ZmSMU2 and AtSMU2 suggests that plant SMU-2 homologues work in a protein complex to regulate not only pre-mRNA splicing but also other aspects of mRNA metabolism. No ZmSMU2-interacting proteins, except ZmSMU1, have human homologues that were previously identified as spliceosomal proteins or are known to function in pre-mRNA splicing (Table II). However, this does not mean that the observed protein interactions conflict with the proposed function of ZmSMU2 in pre-mRNA splicing. Rather, these interactions suggest that ZmSMU2 could also serve as a link to related processes in mRNA metabolism, such as transcription initiation and chromatin modification. Splicing factors, especially SR proteins, were shown to interact with the preinitiation complex, transcription elongation factors, 5′ and 3′ processing factors, and the mRNA export complex (Maniatis and Reed, 2002). In this regard, it is not surprising that ZmSMU2-interacting proteins include proteins that are found in preinitiation complexes. For instance, a Y2H screen for ZmSMU2-interacting proteins identified a partial HAF01 clone (Bertrand et al., 2005) showing a high degree of sequence identity to human $TAF_{II}250$, the largest polypeptide in the TFIID complex. Notably, animal homologues of $TAF_{II}250$ can acetylate histone H4, another ZmSMU2-interacting protein (Mizzen et al., 1996), although it is still unclear whether histone H4 is a genuine in vivo substrate for the histone acetyltransferase activity of $TAF_{II}250$. One intriguing possibility is that SMU2 may mediate coupling of pre-mRNA splicing with chromatin modification. For example, SMU2 could recruit a chromatin modification complex to an alternative exon. Alternatively, SMU2 could help recognize a specific histone code during pre-mRNA splicing and affect alternative splicing of transcripts from genes with a particular chromatin modification (e.g. preferentially include/exclude introns containing a repetitive sequence).

In addition to interacting with a histone or a histone modification factor, ZmSMU2 might also interact with sequence-specific transcription factors in vivo. One of the ZmSMU2-interacting proteins identified in our Y2H screen encodes a protein containing a zinc-coordinating motif and a conserved basic region with high sequence similarity to the Arabidopsis sequence-specific transcription factors AtVOZ1 and AtVOZ2 (Mitsuda et al., 2004). Taken together, protein interactions identified from the Y2H screen suggest a role for ZmSMU2 in connecting pre-mRNA splicing and transcription initiation.

More recently, a biochemical role for animal and plant SMU-1 homologues has been proposed. The human SMU-1 homologue was identified from immunopurified CUL4B-DDB1 ubiquitin ligase complexes (Higa et al., 2006), along with other proteins with a similar type of WD40 motif or DWD (DDB1 binding WD40) motif. These DWD proteins were found to be specific substrate receptors for the corresponding ubiquitin ligase complex. In addition, a subset of Arabidopsis and rice proteins containing a DWD motif was shown to interact with DDB1 in vitro and in vivo

(Lee et al., 2008), although an interaction for AtSMU1 was not tested in this study. Considering the highly conserved interactions of animal and plant DWD proteins with DDB1, plant SMU-1 homologues are most likely involved in the recognition of specific target proteins for ubiquitination. If the proposed CUL4-DDB1-SMU1 ubiquitin ligase complex is involved in proteasome-dependent proteolysis, what can be the target? Probably it is not AtSMU2, since AtSMU2 is unstable in *smu1-2* rather than stabilized (Fig. 2C). Alternatively, the CUL4-DDB1-SMU1 complex may be involved in a nonproteolytic function. No matter what biochemical activity SMU-1 homologues have, their target proteins for ubiquitination are most likely to include spliceosomal proteins.

Comparison of the *C. elegans smu-1* and *smu-2* mutants, the *Atsmu1* and *Atsmu2* mutants, and the *Zmsmu2* mutant indicates that *SMU* orthologues vary in terms of their dispensability. In the nematode, *smu-1* and *smu-2* null mutants are viable and do not show a highly penetrant phenotype (Spike et al., 2001; Spartz et al., 2004), indicating that both loci are dispensable. Genetic interaction between *smu-1* and *smu-2* was also found in *C. elegans*, where these two loci were originally identified from a genetic screen for recessive, loss-of-function *suppressors of mec-8 unc-52* synthetic lethality (Lundquist and Herman, 1994). In the nematode, *smu-1 smu-2* double mutants were phenotypically indistinguishable from the single mutants (Spartz et al., 2004). In Arabidopsis, *smu2* null mutants are viable, while a strong *smu1-1* allele is lethal, and a weak *smu1-2* allele has several developmental defects. In contrast, the maize *smu2* mutants, which are not null, show severe developmental defects and are sterile (Chung et al., 2007), indicating that *Zmsmu2* is an essential gene. Three models could explain the variation among the three species. First, although AtSMU2 and SMU-2 are encoded by single-copy genes, the Arabidopsis and *C. elegans* genomes may encode genes that function in a partially redundant manner to the SMU-2 homologues. Second, although the amino acid sequences of SMU-1 and SMU-2 homologues are highly conserved, these proteins may have diverged to gain additional functions in various eukaryotic organisms. Third, the SMU-1 and SMU-2 homologues may have a similar biochemical role, but their target pre-mRNAs (and proteins if SMU-1 homologues are involved in ubiquitination of target proteins) may differ among various species.

In the last model, ZmSMU2-dependent pre-mRNA targets would be critical for viability, while AtSMU2- and SMU-2-dependent targets may not be as critical for cellular functions to cause early developmental defects. Alternatively, ZmSMU2 may be required for processing of a larger set of pre-mRNA targets than AtSMU2 and SMU-2, and this could result from differences in the respective genomes. For example, the average size of Arabidopsis, rice, and maize introns is estimated to be 167, 413, and 607 bp, respectively (Haberer et al., 2005). This variation in average intron size is probably due to the frequency of transposon insertions in each genome (Haberer et al., 2005). The higher frequency of transposon-related sequences in maize introns could be responsible for the indispensability of ZmSMU2. Consistent with this, transcript profiling of *Zmsmu2-1* endosperm revealed several transposon-like sequences that were differentially expressed in wild-type and *smu2-1* mutant endosperm (Supplemental Table S1). In this regard, it would be interesting to know if *ZmSmu2* is the endosperm splicing regulator that was proposed to be responsible for differential splicing of *waxy* pre-mRNA for the *wxG* allele, which contains a retrotransposon in an intron (Marillonnet and Wessler, 1997). There have been several reports in maize describing similar alternative splicing events that were triggered by insertion of different transposon types, and at least some of the alternative splicing events were found to be tissue specific (Ortiz and Strommer, 1990; Marillonnet and Wessler, 1997; Lal and Hannah, 1999).

MATERIALS AND METHODS

Arabidopsis Mutants

The T-DNA insertional Arabidopsis (*Arabidopsis thaliana*) mutants *smu2-1* (stock identifier SALK_039202), *smu2-2* (stock identifier WiscDsLox320H09), *smu1-1* (stock identifier SALK_123852), *smu1-2* (stock identifier SALK_051163), and *smu1-3* (stock identifier SAIL_95_E04) were obtained from the Arabidopsis Biological Resource Center. The ethyl methanesulfonate mutant *sta1-1* (Lee et al., 2006) was obtained from Dr. Jian-Kang Zhu (University of California, Riverside). *smu2-1* and *smu2-2* were crossed to the Col-0 ecotype twice and *smu1-2* was crossed once before any phenotypic analyses were carried out. Homozygous mutant plants were identified using PCR analysis of genomic DNA isolated from individual plants (Edwards et al., 1991) with a combination of the following primers: for the *AtSMU2-1* allele, 2646Ex7_F_In7 (5′-CCGGTGCCCGAGGTATGTATACTT-3′) and AtMTO_R2 (5′-CTTGGCTCCAAACTGTAAGACCAG-3′); for *Atsmu2-1*, 2646Ex7_F_In7 and T-DNA_LB_b1 (5′-GCGTGGACCGCTTGCTGCAACT-3′); for *AtSMU2-2*, AtMTO_F3 (5′-CCAGTGGATTGTTAAGCCTCAGAC-3′) and 2646In7_R_Ex7 (5′-AAGTATACATACCTCGGGCACCGGGCAG-3′); for *Atsmu2-2*, AtMTO_F3 and pDS-Lox_LB (5′-AACGTCCGCAATGTGTTATTAAGTTGTC-3′); for *AtSMU1-2*, either AtSMU-1_F3 (5′-AGAGTTTCTCATCCGGTAATAGGGAAG-3′) and AtSMU-1_R1 (5′-TCAGGGCTTCCATAACTTCATAGTG-3′) or SMU-4f (5′-TAAATTTCCAGCAACGGTCTCC-3′) and atsmu1-2r (5′-GACATGGCAATAGTCTGGCTAGTACA-3′); for *Atsmu1-2*, either AtSMU-1_F3 and T-DNA_LB_b1 or SMU-4f and LBa1 (5′-TGGTTCACGTAGTGGGCCATCG-3′); for *STA1-1*, AtPRP6_R2 (5′-CCAACTCTCTCACATGCCTCAGCC-3′) and AtPRP6_F2 (5′-AGGGGCTGCGAAGAGTGCCCG-3′); and for *sta1-1*, AtPRP6_R2 and AtPRP6_F2hc (5′-AGAGGGGCTGCGAAGAGAAAAAT-3′).

Characterizations of Mutant Phenotypes

To measure seed weights, four to six plants of the F3 or F4 generation were self-pollinated. All of the F4 plants analyzed were obtained from one of the F3 plants. At least 200 F4 or F5 seeds harvested from each self-pollinated plant were weighed and counted to calculate average seed weights. Seeds were surface sterilized, placed on solid medium (0.5× Murashige and Skoog salts, 1% [w/v] Suc, and 0.7% [w/v] phytoagar), and stored at 4°C for 3 d. Percentage of germination failure or arrested growth, and the number of cotyledons, were analyzed at 7 DAG.

Reporter Constructs and Plant Transformation

For GFP, GUS-GFP, and AtSMU2-GFP fusion proteins, the cDNA for GFP was amplified by PCR using primers *Nco*I_gfpF (5′-CTCACCATGGTGAG-

CAAGGGCGA-3′) and *Bam*HI_gfpR (5′-TAGGATCCTTACTTGTACAGCTCGTC-3′), and the DNA product was digested with *Nco*I and *Bam*HI and introduced into pRTL2 (Carrington et al., 1990). pRTL2 contains two tandem repeats of the cauliflower mosaic virus 35S promoter and the tobacco etch virus leader sequence upstream of multiple cloning sites. The recombinant expression cassette was transferred into the *Hin*dIII site of the binary vector pBIN19 (Bevan, 1984), and the resulting plasmid, pBIN19-35Sp-GFP, was used to transform Arabidopsis Col-0 *gl1* using the floral dip method (Clough and Bent, 1998). To create transgenic Arabidopsis plants expressing *GUS-GFP*, a *GUS* cDNA was amplified with primers *Nco*I_gusF (5′-TCTACCATGGTAGATCTGACTAG-3′) and gusRgfp (5′-TTGCTCACCATGCTAGCTTGTTTGCCTC-3′), and the cDNA for GFP was amplified with primers gusFgfp (5′-AACAAGCTAGCATGGTGAGCAAGGGCGA-3′) and *Bam*HI_gfpR. A second PCR was performed using *Nco*I_gusF and *Bam*HI_gfpR to create the fusion product, *GUS-GFP*. For a transgenic plant overexpressing *AtSMU2-GFP*, the *AtSMU2* cDNA was amplified with primers F+60BspHI (5′-TTTCATGAAACCTTCAAAATCGCATC-3′) and 2646Rgfp (5′-TTGCTCACCATATGCTTGGATCTCTTAG-3′), and the cDNA for GFP was amplified with primers 2646Fgfp (5′-GATCCAAGCATATGGTGAGCAAGGGCGA-3′) and *Bam*HI_gfpR. A second PCR was performed using F+60BspHI and *Bam*HI_gfpR to make the fusion product, *AtSMU2-GFP*. The fusion PCR products, *GUS-GFP* and *AtSMU2-GFP*, were cloned into the *Nco*I and *Bam*HI sites of pRTL2, and the expression cassettes were transferred into the *Hin*dIII site of a binary vector, pBIN19. The resulting plasmids, pBIN19-35Sp-GUS-GFP and pBIN19-35Sp-AtSMU2-GFP, were used to transform Arabidopsis *gl1*. Kanamycin-resistant seedlings were rescued, and images of GFP expressed in roots of the T2 plants at 5 DAG were collected on a Bio-Rad MRC 1024 confocal laser scanning microscope and processed with NIH Image software (http://rsb.info.nih.gov/nih-image/) and Adobe Photoshop 6.0 or CS.

For the *AtSMU1-GFP* translational fusion, a 7.4-kb fragment containing 2.7 kb of 5′ flanking sequence and the coding region of *SMU1* was amplified from Col-0 genomic DNA by Phusion polymerase (Finnzymes) with primers SUM1(−2700)Hind-f (5′-GCTGAAGCTTGGGACATTGAGGCAGC-3′) and SUM1-BamStop-r (5′-GAAGGATCCGGGCTTCCATAACTTCATA-3′), restriction digested with *Hin*dIII and *Bam*HI, and cloned into the pBN-GFP vector (Wang et al., 2006), resulting in construct pBN-SMU1-GFP (*SMU1-GFP*^{Kan}). The *Hin*dIII/*Eco*RI fragment containing *SMU1-GFP* and the nopaline synthase polyadenylation sequence (NOS-ter) was subcloned from pBN-SMU1-GFP into pGPTV-BAR vector (Becker et al., 1992), resulting in construct pGPTV-SMU1-GFP (*SMU1-GFP*^{Bar}).

For complementation of the *Atsmu1-2* mutant, a 7.8-kb fragment containing 2.7 kb of 5′ flanking sequence, the coding region, and 433 bp of 3′ flanking sequence of *SMU1* was amplified from Col-0 genomic DNA by Phusion polymerase with primer SUM1(−2700)Hind-f (5′-GCTGAAGCTTGGGACATTGAGGCAGC-3′) and SUM1-Bam-r (5′-CTGCGGATCCCGTTGTAATGGTCTCTA-3′), restriction digested with *Hin*dIII and *Bam*HI, and cloned into a modified pBI101 vector where the NOS-ter and *GUS* coding regions were replaced with a synthetic linker (5′-GAATTCGAGCTCGGTACCCGGGGATCC-3′), resulting in construct pBI-SMU1 (*SMU1*^{Kan}). The *Hin*dIII/*Eco*RI fragment containing *SMU1* and NOS-ter was subcloned from pBI-SMU1 into pGPTV-BAR vector (Becker et al., 1992), resulting in construct pGPTV-SMU1 (*SMU1*^{Bar}).

The standard flower dip method (Clough and Bent, 1998) was used to transform Arabidopsis ecotype Col-0 or *smu1-2*/+ plants with *Agrobacterium tumefaciens* strain GV3101 pMP90 (Koncz and Schell, 1986) containing appropriate constructs. T1 transformants were selected on Murashige and Skoog medium (Gibco BRL Life Technologies) containing 35 μg mL^{-1} kanamycin or 50 μg mL^{-1} glufosinate ammonium (Crescent Chemical). Kanamycin- or BASTA-resistant plants were transferred to soil, and the presence of the transgene was confirmed by PCR.

Confocal images of the AtSMU1-GFP plants were obtained as described above. Bright-field and epifluorescence images were obtained using a Zeiss Axiophot compound epifluorescence microscope (Carl Zeiss) equipped with a GFP band-pass filter (exciter, 450–490; dichroic, 495; emitter, 500–550 [Chroma Technology]), a fluorescein isothiocyanate long-pass filter (exciter, 450–490; dichroic, 510; emitter, 515 [Carl Zeiss]), a DAPI long-pass filter (exciter, 365; dichroic, 395; emitter, 420 [Carl Zeiss]), and an Optronics MicroFire CCD camera.

Analysis of RNA and Protein

Arabidopsis plants were grown under a 16/8-h light/dark cycle at 20°C. RNA samples were prepared from whole Arabidopsis seedlings grown on solid medium at 14 DAG and roots, leaves, and flowers of Arabidopsis plants grown on soil at 30 DAG.

RNA was isolated using Trizol according to the manufacturer's instructions (Invitrogen). Total RNA was used in a reverse transcription reaction with SuperScript II (Invitrogen) and oligo(dT) primers to generate first-strand cDNA, which was subsequently used to amplify specific cDNAs using standard techniques. Primers for PCR were as follows: for *AtACT8*, AtACT8_F (5′-TAAACTAAAGAGACATCGTTTCCA-3′) and AtACT8_R (5′-TTTTTATCCGAGTTTGAAGAGGCT-3′); for the 5′ coding sequence of *AtSMU2*, AtSMU2_1 (5′-ATGAAACCTTCAAAATCGCATCACAAG-3′) and AtSMU2_2 (5′-AGTCTTCCCACCATCACCATC-3′); for the middle region of the *AtSMU2* coding sequence, AtSMU2_3 (5′-CCAGTGGATTGTTAAGCCTCAGAC-3′) and AtSMU2_4 (5′-CACAGAAGATCCATTCTCAAT-3′); for the 3′ coding sequence of *AtSMU2*, AtSMU2_5 (5′-GAGAAAGATAGGGGTTTGGGA-3′) and AtSMU2_6 (5′-TCAATGCTTGGATCTCTTAGGAGTT-3′); for *AtSRp30*, AtSRp30_F1 (5′-ATGAGTAGCCGATGGAATCGTAC-3′) and AtSRp30_R1 (5′-CAGTTTTCATTTTCAACCAGATATCAC-3′); for *AtTRA2*, AtTRA2_F2 (5′-ATGTCTTACTCAAGAAGGTCAAGA-3′) and AtTRA2_R3 (5′-CGGGGAGAGTAGCTAGGAGACTTA-3′); and for *AtSMU1*, either AtSMU1_1 (5′-AGAGTTTCTCATCCGGTAATAGGGAAG-3′) and AtSMU1_2 (5′-TCAGGGCTTCCATAACTTCATAGTG-3′) or AtSMU1_3 (5′-ACTGAGTACCTCCTTTGACCAAACTGC-3′) and AtSMU1_4 (5′-ACGGAGGTGGCGGCTTGAATGTTTGTA-3′).

For protein extraction, tissues were homogenized in a 2× Laemmli buffer. The extract was centrifuged, and the supernatant was analyzed by SDS-PAGE. Western-blot analysis was conducted as described by Chung et al. (2007).

RNA and protein analyses using maize (*Zea mays*) endosperm extracts were performed as described (Chung et al., 2007). Primers for PCR were as follows: for *rpl15*, ZmrpL15_F1 (5′-AGCCGCATCCGCTATGGGTGCGTA-3′) and ZmrpL15_R2 (5′-CTACCTTTAGGCACAGGCCTCTTCC-3′); for *rpl7a*, ZmrpL7a_F2 (5′-ACGGCCTTAACCATGTGACTTACC-3′) and ZmrpL7a_R3 (5′-CTTGATAGCCTCCAGGATTTTGCT-3′); for *eEf-1α*, ZmEF1a_F2 (5′-TCTCCCCCTACAGGATGTGTACAA-3′) and ZmEF1a_R3 (5′-GCAAACACAGAACCAGCCAGACAC-3′); for *O2* SV1 (major transcript), O2_F1 (5′-ATGGAGCACGTCATCTCAATGGAGG-3′) and O2_R3 (5′-TGGATTCCTTTCTTTTCCTCACTC-3′); for *O2* SV2, O2_F1 and O2_R2a2 (5′-TCCGCTGCTACCCTCCACAT-3′); for *tra2*, ZmTRA2_F1 (5′-ATGTCTTACTCAAGGGGCTCAAGTGA-3′), ZmTRA2_R3 (5′-GATACTTCCCAGGTGTTGGGGTTC-3′), and ZmTRA2_R2a (5′-CAACCCTTTGGCTGAGGTTGGCAT-3′); for *rsp31b*, ZmRSp31B_F2 (5′-AACCCTAGGTCGCCGCCTCTTTTC-3′), ZmRSp31B_R3 (5′-ATGGAAGGAGTTGAAGAGCCCTGG-3′), and ZmRSp31B_R5 (5′-CATCACGTCTACCAGCTTGCTCAC-3′); and for *otux*, ZmOTUX1_F2 (5′-CTATGATGGATACGTTCCCATGGC-3′) and ZmOTUX1_R1 (5′-AAGAGAGCTGAACCCGCCATCAAT-3′).

All RT-PCR and immunoblot analyses were performed with at least three biological replicates. Representative gel images are shown in the figures.

Detection of ZmSMU2-Interacting Proteins with the Y2H System

A full-length *ZmSmu2* cDNA bait sequence for the Y2H screen was prepared by PCR using primers E1 (5′-GGAATTCATGTCATCGAAGAAGAACTACTATAAG-3′) and S1 (5′-TCCCCCGGGGGATCAGCCACGCTGTTTCTTCGAGCT-3′) for insertion between the *Eco*RI and *Sma*I sites of the pBD-GAL4 Cam phagemid vector (Stratagene). Because this construct self-activated in the Y2H system, a series of deletion clones encoding portions of the ZmSMU2 protein were made as follows: the ZmSMU2(I) construct (nucleotides 148–1,698 from the ATG) was created by PCR with primers 38YCONST-I (5′-GGAATTCATGTCGTTTCATGCAGTGGCA-3′) and S1, and the amplified DNA fragment was cloned into pBD-GAL4 between the *Eco*RI and *Sma*I sites; the ZmSMU2(II) construct was created by PCR using primers 38YCONST-II (5′-GGAATTCATGAAAGAAGATCAGGCAGTC-3′) and S1, and the amplified DNA was cloned into pBD-GAL4, as with ZmSMU2(I); the ZmSMU2(III) construct was created by PCR with primers 38YCONST-III (5′-GGAATTCATGCCACCACCACCGGCTCCA-3′) and S1, and the amplified DNA was cloned into pBD-GAL4, as with ZmSMU2(I); the ZmSMU2(IV) construct was created by PCR with primers 38YCONST-IV (5′-GGAATTCATGGGTTATCCAGAACAGTAT-3′) and S1, and the amplified DNA was cloned into pBD-GAL4, as with ZmSMU2(I); the ZmSMU2(V) construct was created by PCR with primers E1 and R4 (5′-CCTGAGTCATGAACCTCGGATC-3′), and the amplified DNA was digested with *Eco*RI and *Eco*RV and inserted into pBD-GAL4, as with ZmSMU2(I). Each construct was verified

using DNA sequencing. The pBD-GAL4-ZmSMU2(IV) construct produced a detectable 5-bromo-4-chloro-3-indolyl-β-D-galactopyranoside product in 2.5 h, and we monitored the yeast colonies for a color reaction that developed within 30 min. On the other hand, deletion of the COOH-terminal 207 amino acids of the ZmSMU2 protein dramatically reduced self-activation in the Y2H system. Consequently, we used the ZmSMU2(V) bait clone to screen maize and Arabidopsis target libraries. Developing maize endosperm (10–14 d after pollination) and immature ear libraries (HybriZAP-2.1 Two-Hybrid Predigested Vector Kit; Stratagene) were obtained from Dr. Bob Schmidt (Department of Biology, University of California San Diego). The Arabidopsis library was from the Arabidopsis Biological Resource Center (http://www.arabidopsis.org/abrc/libraries.jsp; stock no. CD4-22). Yeast transformation and screening procedures were performed according to the manufacturer's instructions. To identify the interacting proteins encoded by Arabidopsis target DNAs, colony PCRs were carried out with primers pACTForward (5′-CTATCTATTCGATGATGAAG-3′) and pACTReverse (5′-ACAGTTGAAGTGAACTTGCG-3′); for maize target genes, the pACTForward and PADT7 (5′-TAATACGACTCACTATAGGG-3′) primers were used. The amplified PCR product was inserted into the pCR4-TOPO vector (Invitrogen) for DNA sequencing.

Expression of Recombinant Proteins in *Escherichia coli* and in Vitro Pull-Down Assays

The following PCR primers were used to produce target proteins fused with a 6XHis tag: for histone H4, AtHIS4_F1 (5′-ATGTCAGGAAGAGGAAAGGGAGGAA-3′) and AtHIS4_R1 (5′-TTAACCTCCGAAACCGTAGAGAGT-3′); for AtSMU1, AtSMU-1_F1 (5′-ATGGCGCTCGAAATCGAAGCTC-3′) and AtSMU-1_R1 (5′-TCAGGGCTTCCATAACTTCATAGTG-3′); and for AtMEC8, AtMEC-8_F1 (5′-ATGGCGTATCACCAACCGTACGA-3′) and AtMEC-8_R1 (5′-TTACTCTATATGCATGCCGCCTCG-3′). The RT-PCR products were cloned into pGEMT-Easy (Promega) and subsequently transferred into the *Eco*RI site of pRSET (Invitrogen) and used to transform the BL21(DE3) strain of *E. coli*. For pull-down experiments where GST fusion proteins were used as a bait protein, cell lysates containing the fused target proteins with a 6XHis tag were prepared in lysis buffer (50 mM Tris, pH 8.5, 150 mM NaCl, 1 mM dithiothreitol, 1 mM EDTA, and 0.2 mM phenylmethanesulfonyl fluoride) containing 1% (v/v) Triton X-100. Purification of GST and GST-ZmSMU2 was performed as described by Chung et al. (2007). Cell lysates containing 0.1 to 0.5 μg of target proteins were preincubated with 0.5 μg of GST and 50 μL of a 50% (v/v) glutathione-agarose slurry (Sigma) at 4°C for 1 h. The cleared cell lysates were added to 50 μL of a 50% (v/v) glutathione-agarose slurry and 10 μg of GST, GST-AtSMU2, or GST-ZmSMU2 protein. The mixtures were adjusted to 1 mL with lysis buffer and incubated at 4°C for 2 h. The beads were then washed four times with lysis buffer containing 0.1% (v/v) Triton X-100. Proteins were eluted in 1× Laemmli sample buffer containing 10 mM glutathione, separated by SDS-PAGE, and transferred onto nitrocellulose membrane. Immunoblot analysis was performed with mouse HisG antibodies (Sigma) at 1:3,000 dilution and then with goat anti-mouse IgG antibodies conjugated with horseradish peroxidase (Sigma) at 1:80,000 dilution.

Supplemental Data

The following materials are available in the online version of this article.

Supplemental Figure S1. Microarray data analysis of *Zmsmu2-1* endosperm.

Supplemental Figure S2. Semiquantitative RT-PCR analysis of RNAs corresponding to coregulated and consistent SP classes of differentially hybridized probes (DHPs) identified in the microarray experiment.

Supplemental Table S1. List of DHP-Hs and DHP-Ls (Microsoft Excel file).

Supplemental Table S2. Correlation of random probes and DHP-L with the number of SVs in MAGI.

Supplemental Table S3. Identification of hybridization sites for random probes and DHP-L, according to the ab initio prediction-based exons and introns in MAGI.

Supplemental Table S4. Identification of hybridization sites for random probes and DHP-L, according to EST-based gene annotation in MAGI.

Supplemental Protocol S1. Results and methods for *Zmsmu2-1* microarray.

ACKNOWLEDGMENT

We thank colleagues in the Larkins laboratory for review and editing of the manuscript.

Received May 22, 2009; accepted August 31, 2009; published September 4, 2009.

LITERATURE CITED

Alonso JM, Stepanova AN, Leisse TJ, Kim CJ, Chen HM, Shinn P, Stevenson DK, Zimmerman J, Barajas P, Cheuk R, et al (2003) Genome-wide insertional mutagenesis of Arabidopsis thaliana. Science **301:** 653–657

Amrein H, Gorman M, Nothiger R (1988) The sex-determining gene Tra-2 of Drosophila encodes a putative RNA-binding protein. Cell **55:** 1025–1035

Becker D, Kemper E, Schell J, Masterson R (1992) New plant binary vectors with selectable markers located proximal to the left T-DNA border. Plant Mol Biol **20:** 1195–1197

Bell LR, Horabin JI, Schedl P, Cline TW (1991) Positive autoregulation of Sex-lethal by alternative splicing maintains the female determined state in Drosophila. Cell **65:** 229–239

Bertrand C, Benhamed M, Li YF, Ayadi M, Lemonnier G, Renou JP, Delarue M, Zhou DX (2005) Arabidopsis HAF2 gene encoding TATA-binding protein (TBP)-associated factor TAF1, is required to integrate light signals to regulate gene expression and growth. J Biol Chem **280:** 1465–1473

Bessonov S, Anokhina M, Will CL, Urlaub H, Luhrmann R (2008) Isolation of an active step I spliceosome and composition of its RNP core. Nature **452:** 846–850

Bevan M (1984) Binary Agrobacterium vectors for plant transformation. Nucleic Acids Res **12:** 8711–8721

Black DL (2003) Mechanisms of alternative pre-messenger RNA splicing. Annu Rev Biochem **72:** 291–336

Brown JWS, Simpson CG (1998) Splice site selection in plant pre-mRNA splicing. Annu Rev Plant Physiol Plant Mol Biol **49:** 77–95

Carrington JC, Freed DD, Oh CS (1990) Expression of potyviral polyproteins in transgenic plants reveals 3 proteolytic activities required for complete processing. EMBO J **9:** 1347–1353

Chung T, Kim CS, Nguyen HN, Meeley RB, Larkins BA (2007) The maize Zmsmu2 gene encodes a putative RNA-splicing factor that affects protein synthesis and RNA processing during endosperm development. Plant Physiol **144:** 821–835

Clough SJ, Bent AF (1998) Floral dip: a simplified method for Agrobacterium-mediated transformation of Arabidopsis thaliana. Plant J **16:** 735–743

Edwards K, Johnstone C, Thompson C (1991) A simple and rapid method for the preparation of plant genomic DNA for PCR analysis. Nucleic Acids Res **19:** 1349

Graveley BR (2000) Sorting out the complexity of SR protein functions. RNA **6:** 1197–1211

Gupta S, Wang BB, Stryker GA, Zanetti ME, Lal SK (2005) Two novel arginine/serine (SR) proteins in maize are differentially spliced and utilize non-canonical splice sites. Biochim Biophys Acta **1728:** 105–114

Haberer G, Young S, Bharti AK, Gundlach H, Raymond C, Fuks G, Butler E, Wing RA, Rounsley S, Birren B, et al (2005) Structure and architecture of the maize genome. Plant Physiol **139:** 1612–1624

Hartmuth K, Urlaub H, Vornlocher HP, Will CL, Gentzel M, Wilm M, Luhrmann R (2002) Protein composition of human prespliceosomes isolated by a tobramycin affinity-selection method. Proc Natl Acad Sci USA **99:** 16719–16724

Higa LA, Wu M, Ye T, Kobayashi R, Sun H, Zhang H (2006) CUL4-DDB1 ubiquitin ligase interacts with multiple WD40-repeat proteins and regulates histone methylation. Nat Cell Biol **8:** 1277–1283

Isshiki M, Tsumoto A, Shimamoto K (2006) The serine/arginine-rich

protein family in rice plays important roles in constitutive and alternative splicing of pre-mRNA. Plant Cell **18:** 146–158

Jumaa H, Nielsen PJ (1997) The splicing factor SRp20 modifies splicing of its own mRNA and ASF/SF2 antagonizes this regulation. EMBO J **16:** 5077–5085

Jurica MS, Licklider LJ, Gygi SP, Grigorieff N, Moore MJ (2002) Purification and characterization of native spliceosomes suitable for three-dimensional structural analysis. RNA **8:** 426–439

Jurica MS, Moore MJ (2003) Pre-mRNA splicing: awash in a sea of proteins. Mol Cell **12:** 5–14

Kalyna M, Lopato S, Barta A (2003) Ectopic expression of atRSZ33 reveals its function in splicing and causes pleiotropic changes in development. Mol Biol Cell **14:** 3565–3577

Koncz C, Schell J (1986) The promoter of T_L-DNA gene 5 controls the tissue-specific expression of chimaeric genes carried by a novel type of Agrobacterium binary vector. Mol Genet Genomics **204:** 383–396

Kumar S, Lopez AJ (2005) Negative feedback regulation among SR splicing factors encoded by Rbp1 and Rbp1-like in Drosophila. EMBO J **24:** 2646–2655

Lal SK, Hannah LC (1999) Maize transposable element Ds is differentially spliced from primary transcripts in endosperm and suspension cells. Biochem Biophys Res Commun **261:** 798–801

Lee BH, Kapoor A, Zhu JH, Zhu JK (2006) STABILIZED1, a stress-upregulated nuclear protein, is required for pre-mRNA splicing, mRNA turnover, and stress tolerance in *Arabidopsis*. Plant Cell **18:** 1736–1749

Lee JH, Terzaghi W, Gusmaroli G, Charron JBF, Yoon HJ, Chen HD, He YJ, Xiong Y, Deng XW (2008) Characterization of *Arabidopsis* and rice DWD proteins and their roles as substrate receptors for CUL4-RING E3 ubiquitin ligases. Plant Cell **20:** 152–167

Lopato S, Forstner C, Kalyna M, Hilscher J, Langhammer U, Indrapichate K, Lorkovic ZJ, Barta A (2002) Network of interactions of a novel plant-specific Arg/Ser-rich protein, atRSZ33, with atSC35-like splicing factors. J Biol Chem **277:** 39989–39998

Lopato S, Kalyna M, Dorner S, Kobayashi R, Krainer AR, Barta A (1999) atSRp30, one of two SF2/ASF-like proteins from Arabidopsis thaliana, regulates splicing of specific plant genes. Genes Dev **13:** 987–1001

Lundquist EA, Herman RK (1994) The mec-8 gene of Caenorhabditis elegans affects muscle and sensory neuron function and interacts with 3 other genes: unc-52, smu-1 and smu-2. Genetics **138:** 83–101

Lundquist EA, Herman RK, Rogalski TM, Mullen GP, Moerman DG, Shaw JE (1996) The mec-8 gene of C. elegans encodes a protein with two RNA recognition motifs and regulates alternative splicing of unc-52 transcripts. Development **122:** 1601–1610

Makarov EM, Makarova OV, Urlaub H, Gentzel M, Will CL, Wilm M, Luhrmann R (2002) Small nuclear ribonucleoprotein remodeling during catalytic activation of the spliceosome. Science **298:** 2205–2208

Makarova KS, Aravind L, Koonin EV (2000) A novel superfamily of predicted cysteine proteases from eukaryotes, viruses and Chlamydia pneumoniae. Trends Biochem Sci **25:** 50–52

Maniatis T, Reed R (2002) An extensive network of coupling among gene expression machines. Nature **416:** 499–506

Marillonnet S, Wessler SR (1997) Retrotransposon insertion into the maize waxy gene results in tissue-specific RNA processing. Plant Cell **9:** 967–978

Mitsuda N, Hisabori T, Takeyasu K, Sato MH (2004) VOZ: isolation and characterization of novel vascular plant transcription factors with a one-zinc finger from Arabidopsis thaliana. Plant Cell Physiol **45:** 845–854

Mizzen CA, Yang XJ, Kokubo T, Brownell JE, Bannister AJ, Owen-Hughes T, Workman J, Wang L, Berger SL, Kouzarides T, et al (1996) The TAF(II)250 subunit of TFIID has histone acetyltransferase activity. Cell **87:** 1261–1270

Neubauer G, King A, Rappsilber J, Calvio C, Watson M, Ajuh P, Sleeman J, Lamond A, Mann M (1998) Mass spectrometry and EST-database searching allows characterization of the multi-protein spliceosome complex. Nat Genet **20:** 46–50

Ortiz DF, Strommer JN (1990) The Mul Maize transposable element induces tissue-specific aberrant splicing and polyadenylation in 2 Adh1 mutants. Mol Cell Biol **10:** 2090–2095

Pazman C, Mayes CA, Fanto M, Haynes SR, Mlodzik M (2000) Rasputin, the Drosophila homologue of the RasGAP SH3 binding protein, functions in Ras- and Rho-mediated signaling. Development **127:** 1715–1725

Rappsilber J, Ryder U, Lamond AI, Mann M (2002) Large-scale proteomic analysis of the human spliceosome. Genome Res **12:** 1231–1245

Reddy ASN (2001) Nuclear pre-mRNA splicing in plants. Crit Rev Plant Sci **20:** 523–571

Reddy ASN (2004) Plant serine/arginine-rich proteins and their role in pre-mRNA splicing. Trends Plant Sci **9:** 541–547

Smith CWJ, Valcarcel J (2000) Alternative pre-mRNA splicing: the logic of combinatorial control. Trends Biochem Sci **25:** 381–388

Spartz AK, Herman RK, Shaw JE (2004) SMU-2 and SMU-1, Caenorhabditis elegans homologs of mammalian spliceosome-associated proteins RED and fSAP57, work together to affect splice site choice. Mol Cell Biol **24:** 6811–6823

Spike CA, Shaw JE, Herman RK (2001) Analysis of smu-1, a gene that regulates the alternative splicing of unc-52 pre-mRNA in Caenorhabditis elegans. Mol Cell Biol **21:** 4985–4995

Wang BB, Brendel V (2006) Genomewide comparative analysis of alternative splicing in plants. Proc Natl Acad Sci USA **103:** 7175–7180

Wang D, Tyson MD, Jackson SS, Yadegari R (2006) Partially redundant functions of two SET-domain polycomb-group proteins in controlling initiation of seed development in Arabidopsis. Proc Natl Acad Sci USA **103:** 13244–13249

Wollerton MC, Gooding C, Wagner EJ, Garcia-Blanco MA, Smith CWJ (2004) Autoregulation of polypyrimidine tract binding protein by alternative splicing leading to nonsense-mediated decay. Mol Cell **13:** 91–100

Xiong LM, Gong ZZ, Rock CD, Subramanian S, Guo Y, Xu WY, Galbraith D, Zhu JK (2001) Modulation of abscisic acid signal transduction and biosynthesis by an Sm-like protein in Arabidopsis. Dev Cell **1:** 771–781

Zhou ZL, Licklider LJ, Gygi SP, Reed R (2002) Comprehensive proteomic analysis of the human spliceosome. Nature **419:** 182–185